Electronic Supplementary Material (ESI) for Lab on a Chip.

Supplementary Information:

Leveraging the Elastic Deformability of Polydimethylsiloxane Microfluidic Channels for Efficient Intracellular Delivery

Hashim Alhmoud[1,2], Mohammed Alkhaled[1,2], Batuhan E. Kaynak[1,2], and M. Selim Hanay[1,2]

1 Department of Mechanical Engineering, Bilkent University, 06800 Ankara, Turkey

2 Institute of Materials Science and Nanotechnology (UNAM), Bilkent University, 06800 Ankara, Turkey

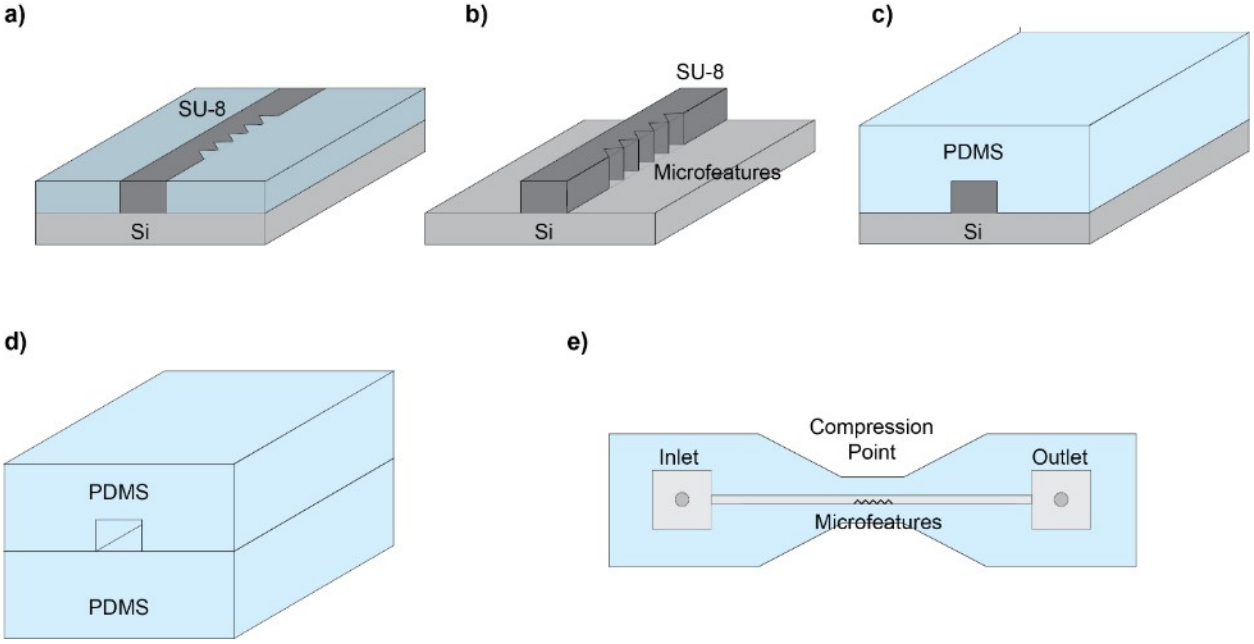

Figure S1: Schematic diagram showing the fabrication of the PDMS device. a) A 100 µm layer of SU-8 photoresist is spun-coated uniformly on a flat silicon wafer. The SU-8 layer is exposed to UV light through a photolithography mask to define the negative of the microfluidic channel with a 100 µm width. The micro-features are defined within the compression region on the photolithography mask at this stage. b) The wafer is hard-baked at 65°C for 15 min and the unexposed SU-8 is dissolved by immersion into SU-8 developer for 10-15 min. c) A mixture of 15:1 PDMS:cross-linker is uniformly coated to the top of the wafer to a thickness of 1 mm. The PDMS is then degassed in a vaccum chamber and then allowed to cure at 95°C for 40 min on a hotplate. Once the PDMS is cured, it is carefully pealed off the silicon wafer. This forms the top layer of the device and includes the engraving of the channel defined by the cross-linked SU-8. At this stage 1.25 mm holes are punched through at either end of the channel to form the inlet and outlet. d) Another completely flat 1 mm PDMS layer using the same 15:1 ratio is prepared to form the bottom layer of the device. Both layers of the device are oxidized in O_2 plasma and then bonded together under vaccum, and then cured at 95°C for 40 min. e) Once the device is completely bonded, it is tested for leaks and then cut out into a dog-bone shape using a stensil ensuring that the micro-features occupy the middle-point of the narrow region of the dog-bone to form the compression region.

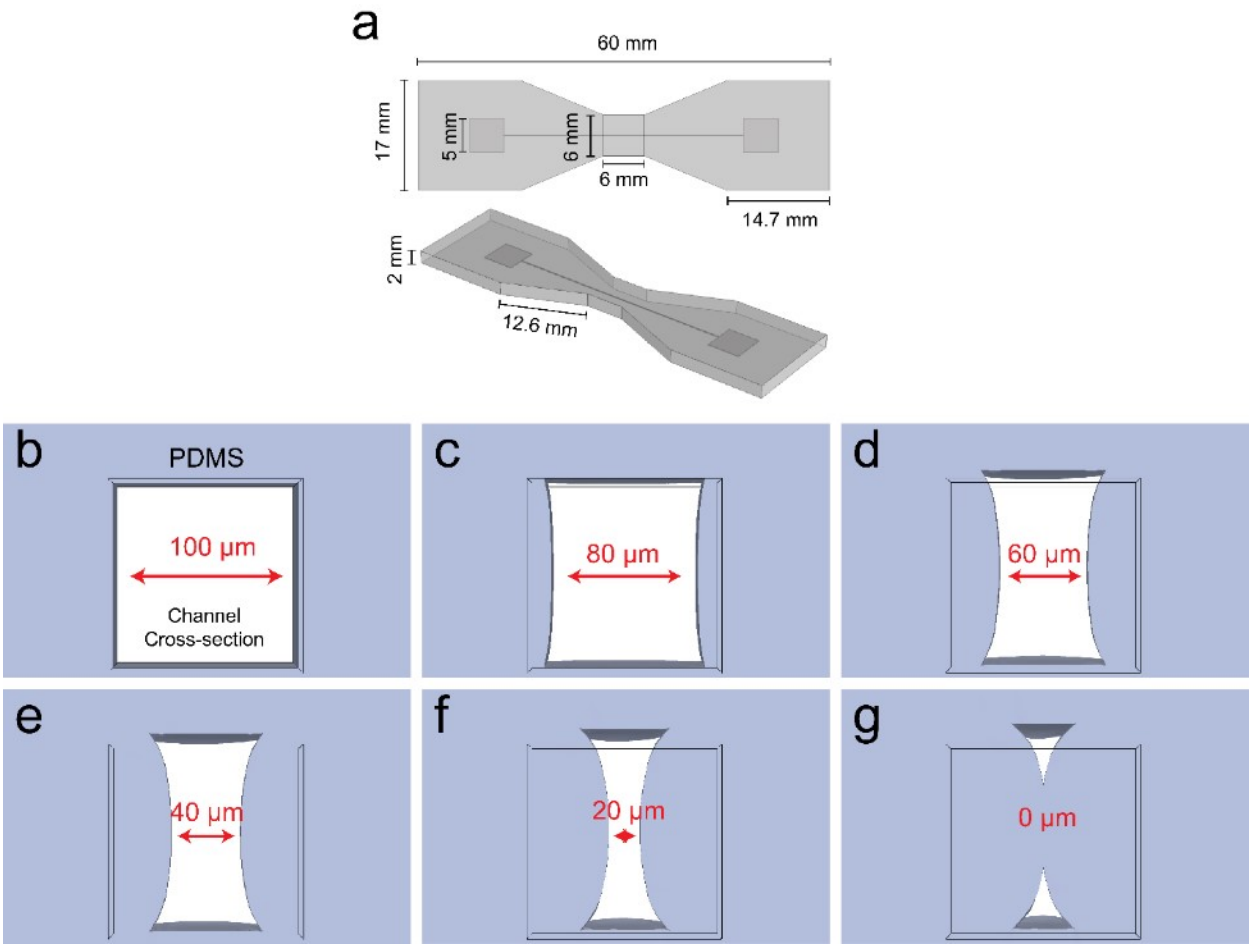

Figure S2: Panel (a) schematic describing the exact dimensions of the PDMS device used in the experiments. Panels (b-g) is a rendered cross-sectional view of the channel at the center of the compression region obtained through simulation. The successive panels show the bulging profile of the channel sidewalls as the external mechanical force is increased. This is a byproduct of the top and bottom of the sidewalls being geometrically fixed to the ceiling and floor of the microfluidic channel, and with any vertical translation being blocked. Even with the channel fully closed, there remains two open portions at the top and bottom (g) that will sustain a small amount of fluid flow (i.e. even when the channel is fully closed, we observe a small flowrate < 1 µL/min flowing through the channel outlet).

S1. Channel sidewall and microfeature bulging

Channel compression is accompanied by non-uniform PDMS deformation caused by compression exclusively along a single axis. This asymmetrical compression necessitates elongation of the PDMS material along the other axes due to Poisson effect. The simulated model shows the emergence of this effect in Figure S3a, where after a certain degree of compression along the axis perpendicular to the channel, the micro-features themselves exhibit elongation along the axis parallel to the channel.

The other major consequence of this effect is the bulging of the channel sidewalls that occurs in a convex manner towards the center of the channel and is exacerbated by increasing the compression force. By looking at the 3D model of the compression region (Figure S3b), we notice that the concave bulging affects both the larger and smaller micro-features (referred to as w_1 and w_2 respectively), with the point of maximum bulging forming the minimum constriction size at the center of the microfeature - denoted as $w_{1,\,min}$ and $w_{2,\,min}$. The maximum constriction size with the least bulging located above and below the maximum bulging region is denoted as $w_{1,\,max}$ and $w_{2,\,max}$.

Given that the bulged constriction can be regarded as parabolically shaped, it is more useful to define $w_{1,\,max}$ as the distance between the w_1 microfeature and the opposing sidewall at the point where the center of a spherically shaped cell touching the top of the channel is located. This is more clearly illustrated in Figure S3c where both $w_{1,\,max}$ and $w_{1,\,min}$ are defined in relation where a given cell is transitioning through the constriction. Based on a parametric sweep of the various displacements of the PDMS device constriction from a fully open state to a closed state where $w_{1,\,min}$ = 0 µm, it was possible to establish a linear relationship between $w_{1,\,min}$ and $w_{1,\,max}$ (Figure S3d) where when $w_{1,\,min}$ = 0, $w_{1,\,max}$ = 16.86 µm. Any increase in $w_{1,\,min}$ is accompanied by a proportional increase in $w_{1,\,max}$ following the equation of the line. This is visualized in the simulated cross-sections of the w_1 constriction region shown in Figure S3e-l. Additional compression beyond the point where $w_{1,\,min}$ = 0 µm leads to a decrease in $w_{1,\,max}$ tending towards full closure of the channel.

The implication of this bulging behaviour on cell membrane permeation is that unlike traditional static constriction systems, cells within the dynamically changeable constriction experience a non-uniform compression as they traverse the constriction region along the height of the channel. For example, an average mammalian cell 14 µm in diameter traversing the constriction where $w_{1,\,min}$ = 10 µm will encounter an effective constriction size ranging from 10-23 µm. This might decrease the yield of cells experiencing sufficient compression to permeabilize the cellular membrane and therefore decrease the efficiency of intracellular delivery. Decreasing the constriction size of w_1 from 50 to 20 µm during fabrication will reduce the extent of bulging when $w_{1,\,min}$ = 0 µm under compression, but that runs the risk of developing non-reversible channel clogging due to the reduced open channel diameter.

Overall, given that the relationship between $w_{1,\,min}$ and $w_{1,\,max}$ is linearly predictable, the rate of membrane permeation at each $w_{1,\,min}$ can be thought of as constant over a statistically large enough sample ($\approx 10^6$ cells/mL) for the purposes of intracellular delivery. Therefore, this non-uniform constriction geometry leading to a decrease in delivery efficiency is a fair compromise to the many advantages offered by a dynamically controllable microfluidic constriction and is an unavoidable consequence of mechanical deformation of materials.

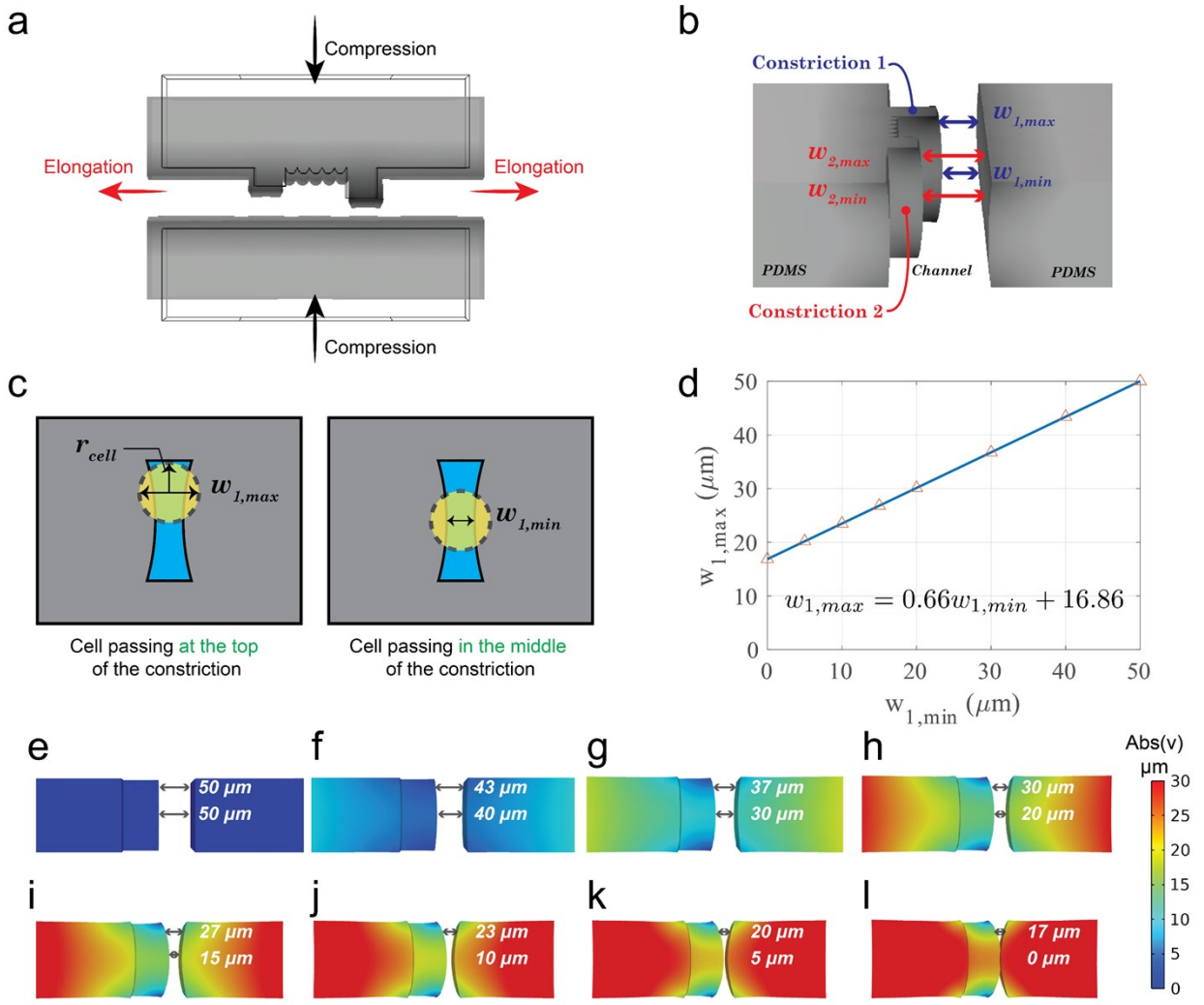

Figure S3: a) representation of the elongation experienced by the channel walls under compression. The solid line frames represent the shape of the constriction region before the application of mechanical force. b) a 3D view of the constriction region under partial compression, showing the bulging that is occurring as a result of channel deformation where w_{min} shows the region with the most bulging (and smaller constriction size), and w_{max} shows the region with the least bulging due to asymmetrical deformation. c) schematics showing the possible routes through which a cell traverses the constriction at the w_1 micro-feature. If the cell has radius = r_{cell}, then $w_{1,\,max}$ is defined as the distance between the micro-feature and the opposite sidewall at a distance of r_{cell} from the top or the bottom of the channel. d) graph showing the linear relationship between $w_{1,\,min}$ and $w_{1,\,max}$ for a cell with radius r_{cell} = 7 μm as derived from the simulation. e-l) are heatmaps of the w_1 constriction cross-section showing the displacement caused by applying mechanical force. The top number in each case shows the value of $w_{1,\,max}$ while the bottom number refers to the value of $w_{1,\,min}$.

S2. Accurate constriction measurement during experimentation

In the previous section, it was established that the channel sidewalls undergo bulging as more compressive force is applied from the outside. This effect when viewed under the microscope appears as out-of-focus dark shadows surrounding the sharp edges of the micro-features and the channel sidewalls (Figure 2j-o). As more compression is applied, those dark regions extending from the channel sidewalls begin to visually merge with dark regions extending from the opposite part of the channel. This visual effect hinders accurate constriction measurement when the most prominent micro-feature (w_1) is less than 15 μm from the opposite channel sidewall.

Since accurate constriction measurement is essential for establishing a relationship between minimum constriction size ($w_{1,\,min}$, Figure S4a) and the efficiency of intracellular delivery, a method for measuring $w_{1,\,min}$ accurately under a microscope was used for all subsequent experiments.

In this method, the distance of the edge of w_2 from the opposite sidewall is measured as a proxy to determine the corresponding distance of w_1 and the constriction size. This is possible since the change in both distances is linear. The distance from w_2 to the opposite wall is clearer to measure since its edge is farther away from the opposing sidewall by ~20 μm. Using the numerical simulation, we accurately calculated the minimum distance ($w_{2,\,min}$) from the opposing sidewall as a function of $w_{1,\,min}$ which resulted in a linear relationship with the following equation of the line (Figure S4):

$$w_{1,min} = 0.94 w_{2,min} - 15.8$$

Empirical measurements of both constrictions under a microscope aligned very well with the line derived from the simulation except for values of $w_{1,\,min} < 20$ μm where the datapoints showed a deviation towards smaller $w_{2,\,min}$ values due to errors in $w_{1,\,min}$ measurements. Therefore, for all subsequent measurements, $w_{1,\,min}$ was calculated by measuring $w_{2,\,min}$ experimentally and deriving the value of $w_{1,\,min}$ from the linear equation established in the simulation to obtain an accurate constriction size measurement.

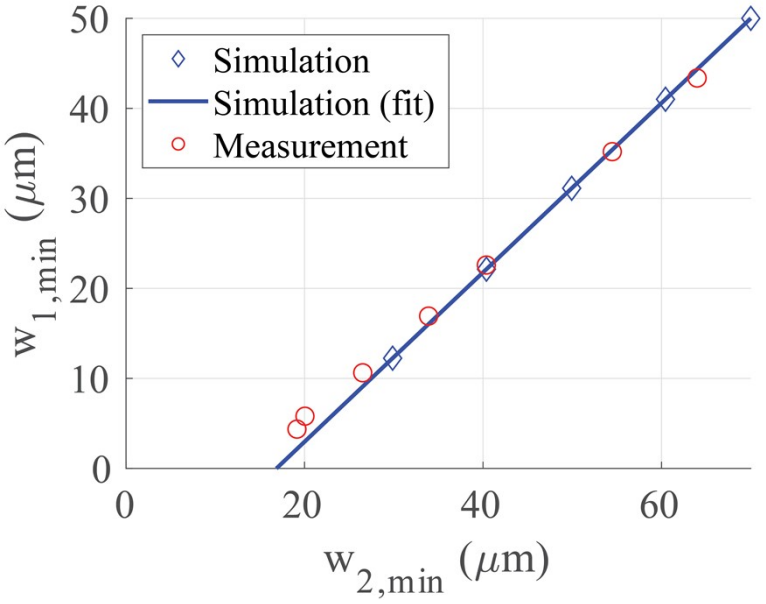

Figure S4: Graph showing the relationship between $w_{1,\,min}$ and $w_{2,\,min}$ and the equation of the line. The circular datapoints represent real measurements of both constrictions carried out under a microscope under various compression forces. The plot shows good agreement ($R^2 = 0.999$) between the simulated line and the empirically measured datapoints.

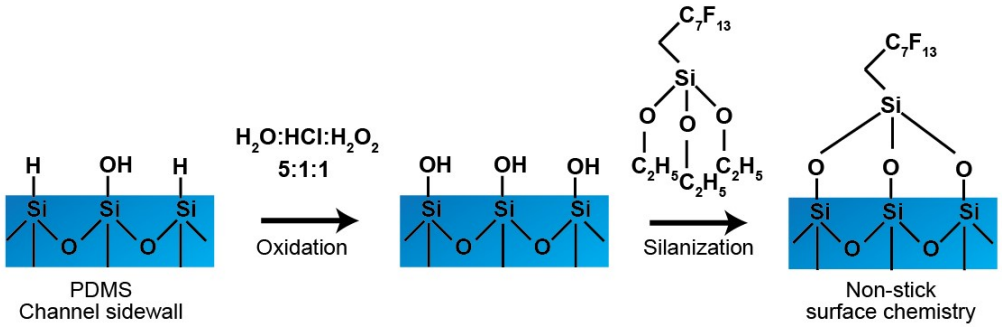

Figure S5: Schematic depicting the reaction scheme used to passivate the surface of the inner walls of the microfluidic channel. The PDMS surface is usually covered with silicon hydride and silicon hydroxide groups. Exposing it to an oxidizing solution of H_2O:HCl:H_2O_2 (5:1:1) will cause the entire surface to become oxidized and silicon hydroxide groups become dominant. The surface is then dried and exposed to 1H, 1H, 2H, 2H-Perfluorooctyltriethoxysilane (4% v/v% in ethanol) for 30 min at room temperature. The reaction leads to the formation of Si-O-Si groups thus covalently bonding the fluorosilane to the surface of the inner walls of the channel. The long fluorocarbon chain (-C_7F_{13}) effectively passivates the surface and prevents ionic and Van der Waals interactions with the surface.

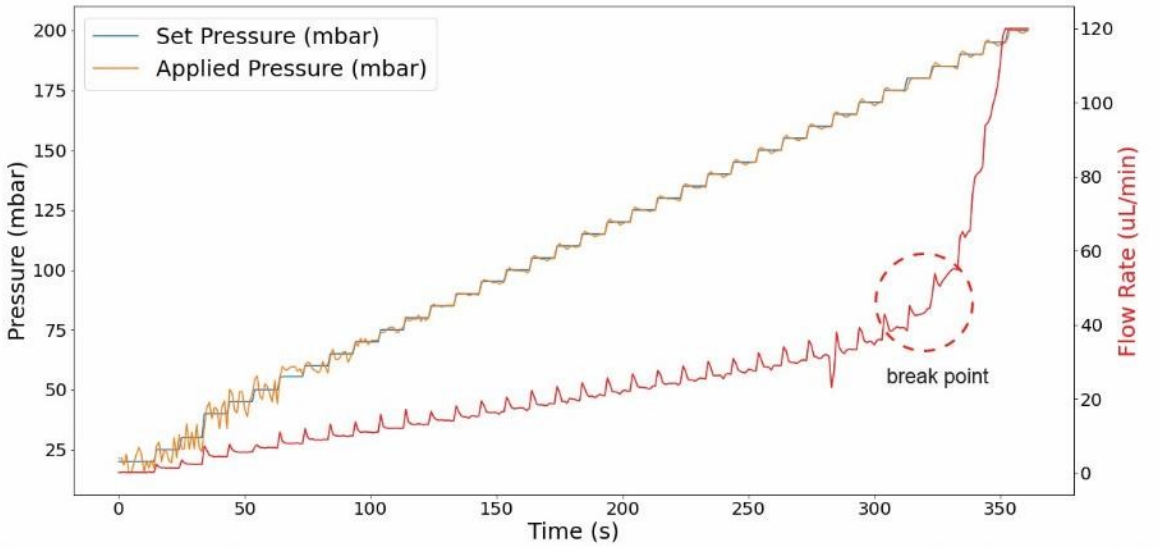

Figure S6: Plot that shows the maximum flowrate tolerated by the PDMS device before developing a leak. The first y-axis describes the pressure (in mbar) applied to a fluid reservoir to push it through the PDMS microfluidic channel (Fluigent) where the set pressure is defined using the controller software, and the applied pressure is what is actually outputted by the air pump. The second y-axis is the output of a flowrate sensor attached between the fluid reservoir and the microfluidic channel. The salient feature of this plot is a clear "break point" where a leak develops between 75 -100 mbar. This is indicated by a sharp increase in the flowrate after 325 s which correlates with a maximum flowrate of ~ 42 µL/min.

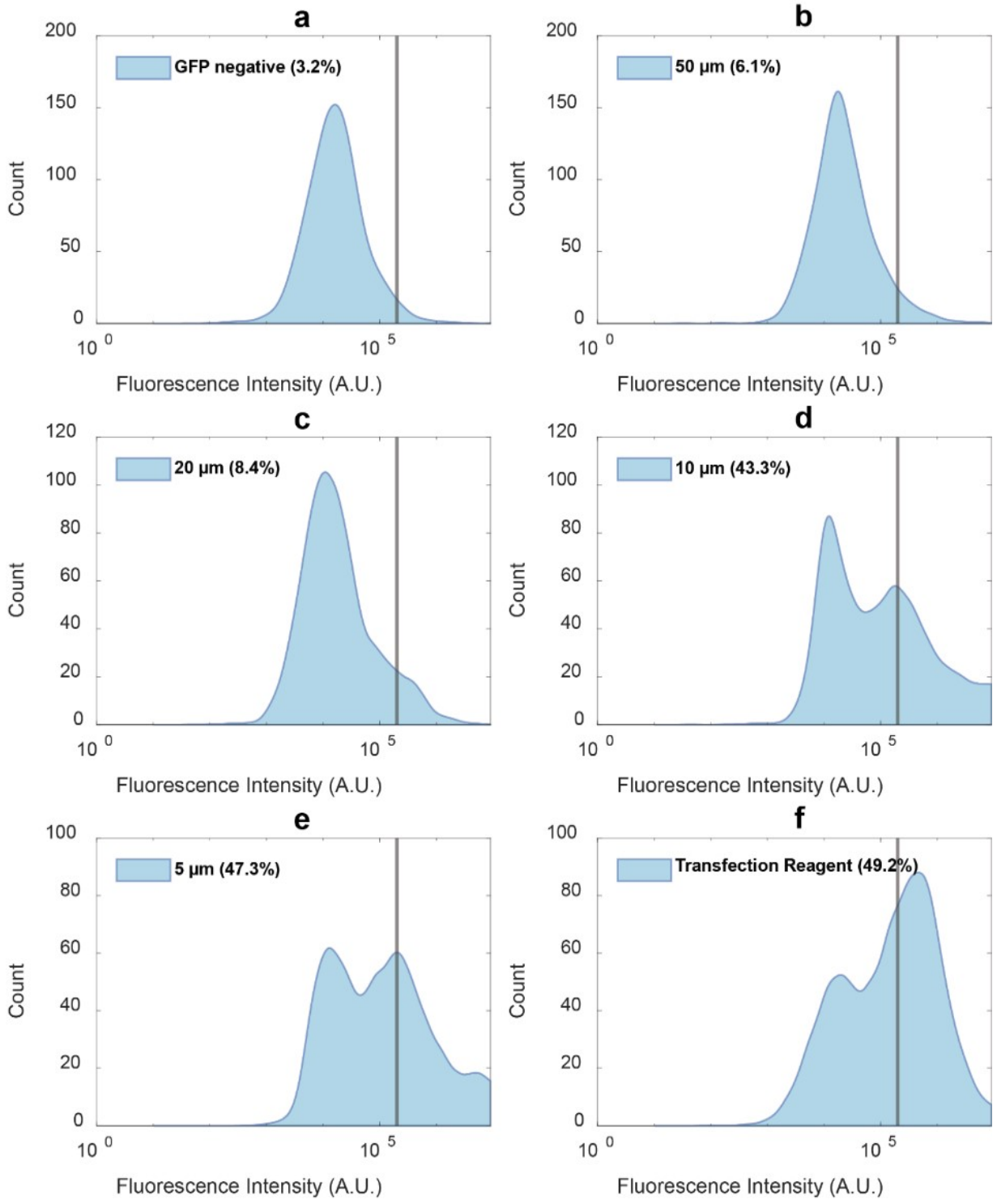

Figure S7: Flow cytometry results of fluorescence in the green channel for HEK293 FT cells treated using the device in the presence of the GFP-coding plasmid. Panel (a) shows the fluorescence of cells not treated with the device to establish a threshold for HEK293 FT background fluorescence, which is indicated by the vertical red line positioned at 2×10^5 A.U. Panels (b-e) represent cells that passed through the PDMS channel at different constriction sizes (50, 20, 10, and 5 µm). Cells that fluoresced with an intensity larger than the established threshold were counted as successfully transfected. The red percentage value in each panel represents the amount of cells with fluorescence above background. Panel (f) shows GFP fluorescence for HEK293 FT cells transfected using a commercial reagent as a positive control.

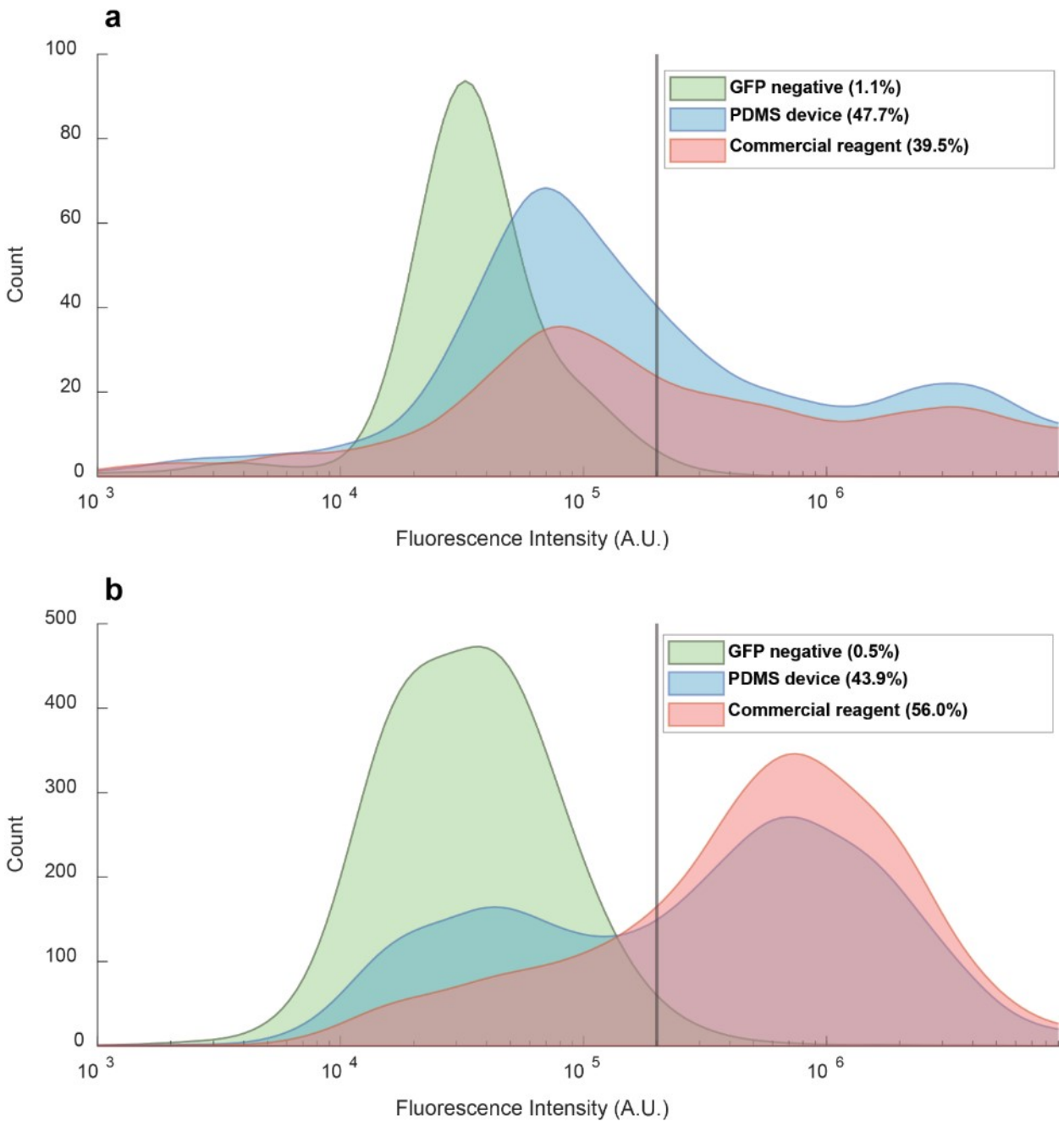

Figure S8: Flow cytometry results of fluorescence in the green channel for (a) MDA MB 231 cells and (b) MCF 7 treated using the device (10 µm constriction size) in the presence of the GFP-coding plasmid. The results are compared to a positive control which is a commercial lipid-based transfection reagent.

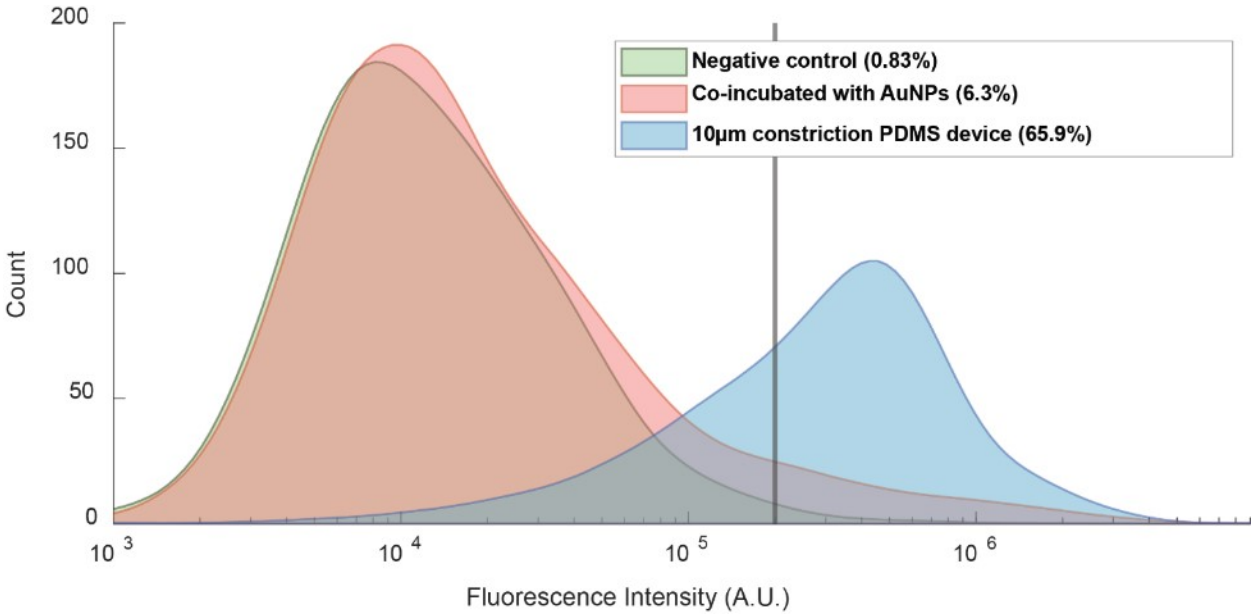

Figure S9: Flow cytometry results of green channel fluorescence for HEK293 FT cells treated with the PDMS device in the presence of GFP-labeled 20 nm AuNPs. Negative control labeled sample (blue) are untreated cells used to establish threshold for significant fluorescence. The co-incubated sample (orange) refers to cells co-incubated with AuNPs but not injected through the device channel. The sample squeezed through 10 µm constriction (green) refers to cells co-incubated with AuNPs and injected into the device channel with a 10 µm constriction.

a

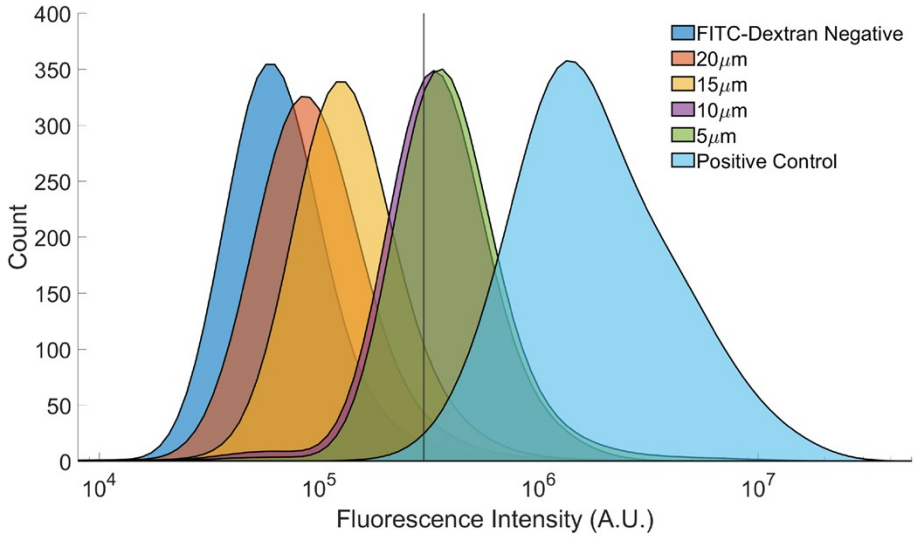
FITC-Dextran Negative
20μm
15μm
10μm
5μm
Positive Control
Count
Fluorescence Intensity (A.U.)

b

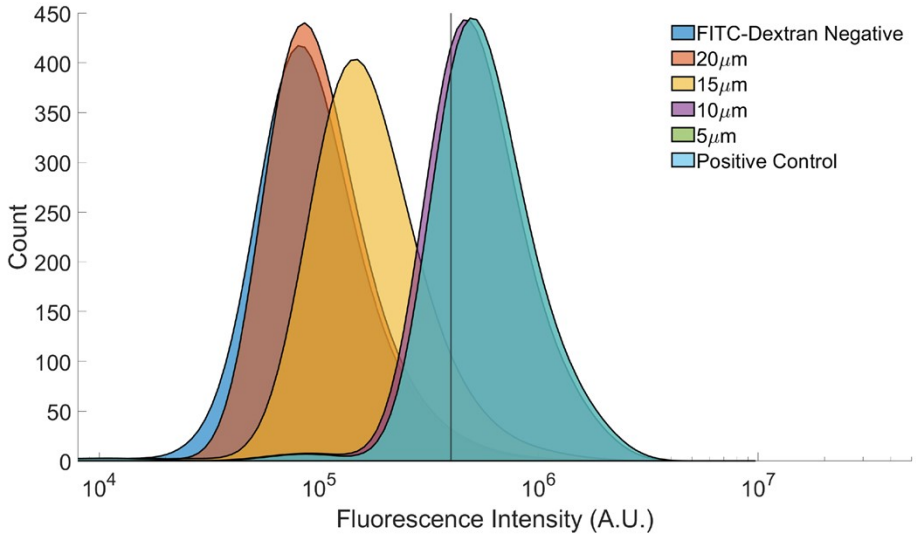
FITC-Dextran Negative
20μm
15μm
10μm
5μm
Positive Control
Count
Fluorescence Intensity (A.U.)

c

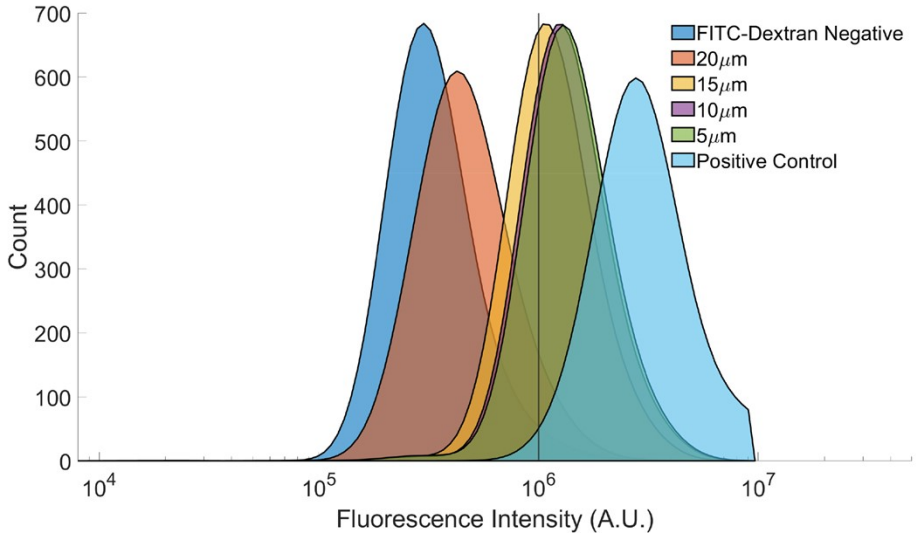
FITC-Dextran Negative
20μm
15μm
10μm
5μm
Positive Control
Count
Fluorescence Intensity (A.U.)

Figure S10: Flow cytometry histograms of green fluorescence intensity of a) HEK293 FT, b) MCF 7, and c) MDA MB 157. Each cell population was flown through 20, 17, 15, 12, 10, 7, and 5 μm minimum constriction sizes ($w_{1,\ min}$) but only 20, 15, 10, and 5 μm constriction sizes are shown to minimize the extent of overlap between the curves. Additionally, data is shown for the FITC-Dextran negative samples to establish background fluorescence limits, and the positive control samples (with chemically permeated membranes) to establish the maximum limits for green fluorescence intensity. The vertical lines in each plot represents the threshold beyond which fluorescence intensity is considered positive based on the negative control.